Staufen1 impairs stress granule formation in skeletal muscle cells from myotonic dystrophy type 1 patients

Aymeric Ravel-Chapuis, Amanda Klein Gunnewiek, Guy Bélanger, Tara E. Crawford Parks, Jocelyn Côté, and Bernard J. Jasmin*
Department of Cellular and Molecular Medicine and Centre for Neuromuscular Disease, Faculty of Medicine, University of Ottawa, Ottawa, ON K1H 8M5, Canada

ABSTRACT **Myotonic dystrophy (DM1) is caused by an expansion of CUG repeats (CUG^{exp}) in the DMPK mRNA 3′UTR. CUG^{exp}-containing mRNAs become toxic to cells by misregulating RNA-binding proteins. Here we investigated the consequence of this RNA toxicity on the cellular stress response. We report that cell stress efficiently triggers formation of stress granules (SGs) in proliferating, quiescent, and differentiated muscle cells, as shown by the appearance of distinct cytoplasmic TIA-1– and DDX3-containing foci. We show that Staufen1 is also dynamically recruited into these granules. Moreover, we discovered that DM1 myoblasts fail to properly form SGs in response to arsenite. This blockage was not observed in DM1 fibroblasts, demonstrating a cell type–specific defect. DM1 myoblasts display increased expression and sequestration of toxic CUG^{exp} mRNAs compared with fibroblasts. Of importance, down-regulation of Staufen1 in DM1 myoblasts rescues SG formation. Together our data show that Staufen1 participates in the inhibition of SG formation in DM1 myoblasts. These results reveal that DM1 muscle cells fail to properly respond to stress, thereby likely contributing to the complex pathogenesis of DM1.**

Monitoring Editor
A. Gregory Matera
University of North Carolina

Received: Jun 11, 2015
Revised: Mar 24, 2016
Accepted: Mar 25, 2016

INTRODUCTION

Myotonic dystrophy type 1 (DM1) is a multisystemic disorder caused by a repetition of CUG trinucleotides in the 3′-untranslated region (3′UTR) of dystrophia myotonica protein kinase (DMPK) mRNA. Pathological severity of the disease correlates with the size of the CUG expansion (CUG^{exp}; Fu *et al.*, 1992; Tsilfidis *et al.*, 1992). CUG^{exp}-containing mRNAs accumulate in cell nuclei, where they form distinct mRNA foci detectable by fluorescence in situ hybridyzation (FISH) with fluorophore-conjugated (CAG)10 probes. CUG^{exp} mRNAs become toxic to cells, as they misregulate expression of multiple RNA-binding proteins. In particular, MBNL1 is sequestered in the nucleus by CUG^{exp} nuclear aggregates, thereby reducing the availability of functional MBNL1 in the rest of the cell (Miller *et al.*, 2000). In contrast, CUGBP1 and Staufen1 expression are increased in vivo in DM1 muscle tissue samples (Savkur *et al.*, 2001; Ravel-Chapuis *et al.*, 2012). The imbalance created in the level of these RNA-binding proteins in turn modifies the pattern of alternative splicing of several pre-mRNAs, thus defining DM1 as a spliceopathy. For example, missplicing of insulin receptor and chloride channel pre-mRNAs is directly linked to the insulin resistance and myotonia seen in DM1 patients, respectively (Savkur *et al.*, 2001; Charlet *et al.*, 2002). RNA-binding proteins that are misregulated in DM1 by CUG^{exp} mRNAs are also known to be multifunctional proteins playing diverse roles in RNA metabolism in addition to pre-mRNA splicing. Indeed, several studies have reported that their misregulation in DM1 also alters miRNA biogenesis, as well as mRNA transport,

This article was published online ahead of print in MBoC in Press (http://www.molbiolcell.org/cgi/doi/10.1091/mbc.E15-06-0356) on March 30, 2016.

A.R.C., A.K.G., G.B., and T.E.C.P. performed the experiments. A.R.C., A.K.G., J.C., and B.J.J. analyzed the data. A.R.C., J.C., and B.J.J. designed the experiments and wrote the manuscript.

*Address correspondence to: Bernard J. Jasmin (jasmin@uottawa.ca).

Abbreviations used: ALS, amyotrophic lateral sclerosis; CHX, cycloheximide; CUG^{exp}, CUG expansion; DM1, myotonic dystrophy type 1; DMPK, dystrophia myotonica protein kinase; eIF, eukaryotic initiation factor; ER, endoplasmic reticulum; FISH, fluorescence in situ hybridyzation; FMRP, fragile X mental retardation protein; FUS, fused in sarcoma; GAPDH, glyceraldehyde-3-phosphate dehydrogenase; G3BP, RasGAP-associated endonuclease; GFP, green fluorescent protein; HS, heat shock; IR, insulin receptor; MyHC, myosin heavy chain; PABP, poly(A)-binding protein; PCC, Pearson's correlation coefficient; qRT-PCR, quantitative reverse transcription PCR; SGs, stress granules; shRNA, short hairpin RNA; SMN, survival of motor neuron; SOD, superoxide dismutase; TDP-43, TAR DNA-binding protein 43; TIA-1, T-cell integral antigen-1; 3′UTR, 3′-untranslated region; WDM, Welander distal myopathy.

stability, and translation efficiency, thereby illustrating the variety of cellular processes affected in DM1 and likely involved in the etiology of the disease (Schoser and Timchenko, 2010; Mahadevan, 2012; Thornton, 2014).

Accumulating evidence indicates that DM1 cells expressing mutant CUG^{exp} mRNAs are exposed to several forms of cellular stress. An increased level of free radicals, accompanied by increased levels in superoxide dismutase (SOD) and other oxidative stress markers, was reported from different cohorts of DM1 patients, showing that DM1 cells are more susceptible to oxidative stress (Ihara *et al.*, 1995; Usuki and Ishiura, 1998; Usuki *et al.*, 2000; Toscano *et al.*, 2005; Kumar *et al.*, 2014). In addition, an increase in endoplasmic reticulum (ER) stress was also observed in DM1 cells, presumably caused by the imbalance in Ca^{2+} homeostasis originating from the missplicing of SERCA and RyR pre-mRNAs (Ikezoe *et al.*, 2007; Botta *et al.*, 2013). These observations raise the question of how DM1 cells cope with stress generated by expression of toxic CUG^{exp} mRNA and how it affects DM1 pathophysiology.

Stress granules (SGs) are large cytoplasmic structures that form in response to a variety of stress conditions, such as oxidative stress, ER stress, heat shock, and viral infection. These granules are dynamic structures exhibiting rapid turnover in which mRNAs are processed for storage, degradation, or reinitiation (Kedersha *et al.*, 2000). SGs are composed of stalled translation initiation complexes containing polyadenylated mRNAs bound to the 48S preinitiation complex, which includes the 40S small ribosomal subunit and early initiation factors such as eukaryotic initiation factor 3 (eIF3), eIF4A, eIF4E, eIF4G, and poly(A)-binding protein (PABP; Anderson and Kedersha, 2008; Buchan and Parker, 2009). Early steps of SG assembly involve the phosphorylation of the translation initiation factor eIF2α (Kedersha *et al.*, 1999). Alternatively, SGs can form through eIF2α phosphorylation-independent pathways (Dang *et al.*, 2006; Mazroui *et al.*, 2006; Farny *et al.*, 2009; Mokas *et al.*, 2009). This is followed by the aggregation of the primary SG nucleators T-cell integral antigen-1 (TIA-1; Kedersha *et al.*, 1999) and RasGAP-associated endonuclease (G3BP; Tourriere *et al.*, 2003). Many other RNA-binding proteins are also recruited to SGs and participate in their aggregation. For example, we and others showed that the DEAD box RNA helicase DDX3 is localized in SGs upon stress induction (Goulet *et al.*, 2008; Lai *et al.*, 2008). DDX3 interacts with eIF4E and PABP1, and its downregulation impairs SG formation, making it a crucial regulator of SG biogenesis (Shih *et al.*, 2012). In addition to proteins directly involved in RNA metabolism, other molecules are also known to localize to SGs. In particular, signaling proteins, including those involved in the induction of apoptosis, are also relocalized to SGs, thereby preventing the activation of cell death during transient stress. Consequently, in the current model, SGs are believed to promote cell survival while facing stress conditions (Kedersha *et al.*, 2013). When cells eventually recover from the undesired stress, SGs disperse, and untranslated mRNAs that accumulated are then rapidly available for translation.

In the present study, we examined the potential of normal muscle cells to form SGs at different stages of differentiation. Moreover, we also studied SG formation in cultured DM1 cells. For this, we assessed how DM1 fibroblasts versus myoblasts respond to stress. Finally, we evaluated the putative function of Staufen1 in DM1 muscle cells and ascertained its role in the formation of SGs.

RESULTS

SGs form in stressed muscle cells in culture

We first assessed the potential of normal muscle cells to respond to stress by forming SGs. SGs form in response to a variety of exogenous stresses and are believed to constitute a cellular protective mechanism. Here we first used arsenite, a drug commonly used to induce oxidative stress in cells. Proliferative mouse C2C12 myoblasts were treated with 0.5 mM sodium arsenite for 45 min and SG formation assessed by immunofluorescence using anti-TIA-1 antibodies, a well-accepted marker of SGs (Kedersha and Anderson, 2007). In normal proliferative mouse myoblasts, TIA-1 showed nuclear localization, accompanied by low, diffuse cytoplasmic staining (Figure 1A). Arsenite-induced stress causes the partial relocalization of TIA-1 in distinct and characteristic cytoplasmic SGs (Figure 1A). Under these conditions, nuclear TIA-1 staining is still observed. We previously showed that DDX3 colocalizes with TIA-1 in SGs in HeLa cells (Goulet *et al.*, 2008). We thus also investigated the localization of DDX3 in muscle cells by coimmunofluorescence. In proliferative mouse myoblasts, DDX3 has a diffuse cytoplasmic staining pattern, whereas in stressed conditions, most of the DDX3 relocalizes to newly formed SGs and displays a subcellular distribution that coincides with that of TIA-1 (Figure 1A). We also performed a colocalization analysis on TIA-1 and DDX3 immunostaining. To this end, we measured the intensity of TIA-1 and DDX3 signals along a line segment crossing SGs (Supplemental Figure S1A). Intensity plots show near-complete overlap in TIA-1 and DDX3 signal intensities, revealing that DDX3 and TIA-1 highly colocalize upon arsenite stress in proliferative mouse skeletal muscle cells. In addition, a high Pearson's r (0.88 ± 0.01) further confirms quantitatively this near-complete colocalization of TIA-1 and DDX3 in cytoplasmic SGs (Figure 1A).

PABP1 associates with the poly(A) tail of mRNAs and with eIF4F and hence is known to play a key role in mRNA metabolism. PABP1 also segregates with SGs upon stress and therefore represents a translation-associated marker of SGs (Kedersha *et al.*, 1999). In our experiments, we observed that PABP1 is mainly cytoplasmic in proliferative myoblasts but relocates to distinct SGs that colocalize to a large extent with TIA-1 (r = 0.87 ± 0.01), confirming the fact that these cytoplasmic aggregates are indeed SGs (Figure 1B).

Other stressors are known to induce SG formation in different cell types. Therefore we tested the susceptibility of myoblasts to respond to other sources of stress in addition to arsenite. C2C12 myoblasts were exposed to heat shock (HS) at 45°C for 45 min, and SG formation was monitored by TIA1 and DDX3 staining. HS induced the formation of many large cytoplasmic TIA1- and DDX3-positive SGs (r = 0.90 ± 0.01; Figure 1A). Finally, another stress, ER stress, which can be induced with thapsigargin (1 µM thapsigargin for 60 min), efficiently triggered the formation of SGs in C2C12 myoblasts (r = 0.93 ± 0.01; Figure 1A).

Staufen1 participates in SG formation in skeletal muscle cells

We previously reported the regulation of Staufen1, a protein involved in key aspects of RNA metabolism, in skeletal muscle cells (Belanger *et al.*, 2003; Ravel-Chapuis *et al.*, 2012, 2014). We thus analyzed the localization of Staufen1 in response to stress in C2C12 myoblasts. By immunofluorescence microscopy, Staufen1 is mainly observed in the cytoplasm in diffuse, as well as in small punctuate, granules (Figure 2A). After arsenite stress, Staufen1 becomes concentrated into large, distinct cytoplasmic aggregates. Coimmunofluorescence experiments showed that these Staufen1-containing granules colocalize with TIA-1 aggregates, revealing that Staufen1 is recruited into SGs (Figure 2A). In our analyses, a linear intensity plot examination showed that Staufen1 and TIA-1 signals overlap in SGs (Supplemental Figure S2A). However, we found that a fraction of Staufen1 also accumulates in a separate, TIA-1–negative domain at the periphery of TIA-1–positive granules (Supplemental Figure S2A). Accordingly, a relatively lower r between TIA-1 and Staufen1 (r = 0.82 ± 0.01) is

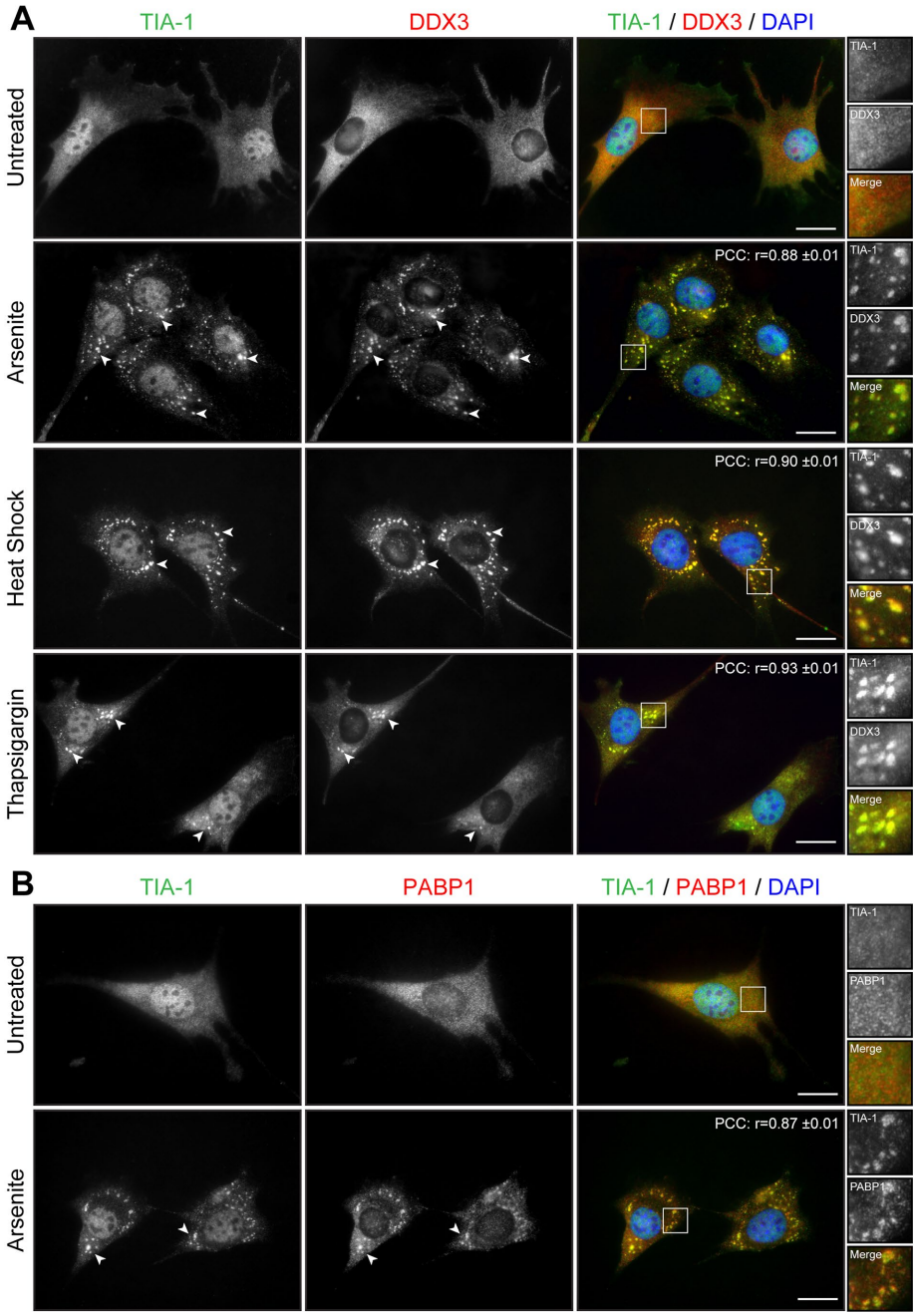

FIGURE 1: Cell stress induces the formation of SGs in myoblasts. (A) Proliferative C2C12 myoblasts were untreated or treated with arsenite (0.5 mM for 45 min), by heat shock (45°C for 60 min), or with thapsigargin (1 μM for 60 min). Coimmunofluorescence stainings were performed using TIA-1 and DDX3 antibodies. (B) Coimmunofluorescence stainings were performed on untreated and arsenite-treated proliferative C2C12 using TIA-1 and PABP1 antibodies. DAPI was used to stain nuclei. Arrowheads show SGs in myoblasts. Right, magnifications of areas outlined by white boxes. Scale bars, 20 μm. For *r*, 40, 12, 11, and 11 cells were analyzed, respectively.

observed than between TIA-1 and DDX3 (see earlier discussion), reflecting partial localization of Staufen1 into SGs (Figure 2A).

It is well established that drugs that stabilize polysomes, such as cycloheximide (CHX), which traps elongating ribosomes on mRNAs, inhibit the assembly of SGs. On the contrary, drugs that destabilize polysomes, such as puromycin, which promote the release of elongating ribosomes, stimulate the assembly of SGs (Kedersha *et al.*, 2000). Concomitantly to arsenite stress, C2C12 myoblasts were treated with either CHX or puromycin. As expected, the formation of TIA-1–positive SGs by arsenite was prevented by the presence of CHX but not puromycin (Figure 2B). From these results, we conclude that mouse myoblasts efficiently form TIA-1/DDX3/Staufen1–positive SGs in response to induced stress.

To study further the relocalization of Staufen1 into SGs during stress, we cotransfected C2C12 cells with Staufen1–green fluorescent protein (GFP) and TIA-1-mCherry constructs. At 48 h after transfection, many transfected cells displayed spontaneous SG formation. This is consistent with previous observations in TIA-1–overexpression experiments (Gilks *et al.*, 2004; Kedersha *et al.*, 2005; Kedersha and Anderson, 2007). Focusing on cells that did not spontaneously form SGs, we observed localization of Staufen1-GFP and TIA-1-mCherry that recapitulates the distribution of endogenous Staufen1 and TIA-1 (compare Figures 2A and 3A). As expected, Staufen1 is recruited into TIA-1–positive granules after arsenite stress treatment. A linear intensity plot analysis together with an *r* matching the one obtained with endogenous proteins ($r = 0.82 \pm 0.01$; see earlier discussion) shows that Staufen1 and TIA-1 signals almost completely overlap in SGs under these conditions. Remarkably, no exogenous Staufen1 accumulates outside of TIA-1-mCherry–positive compartments (compare Figure 3A and Supplemental Figure S2B).

To provide additional insight into the dynamic recruitment of Staufen1 into SGs, we also carried out live-cell imaging on C2C12 cells transfected with Staufen1-GFP and TIA-1-mCherry. Transfected cells were treated with arsenite and imaged every 5 min for 1 h by spinning-disk confocal microscopy. When we followed this over time, we observed concomitant aggregation of Staufen1 into TIA-1 after 25–30 min of arsenite treatment. Thereafter Staufen1 and TIA1 remained colocalized for the rest of the duration of the treatment, whereas SGs keep aggregating (Figure 3B and Supplemental Videos S1 and S2). Some cells displayed preformed cytoplasmic Staufen1-aggregates as observed with endogenous Staufen1 (compare Figures 2A and 3B). These aggregates remained separate entities or partially redistributed after arsenite treatment into newly formed TIA-1 granules (Figure 3B and Supplemental Videos S1 and S2). Taken together, these data indicate that Staufen1 localization is compatible with a role in both dynamic assembly and structural maintenance of SGs.

SGs form in differentiated mature muscle cells

We next studied whether the state of differentiation of muscle cells influences SG formation. A decrease in serum concentration

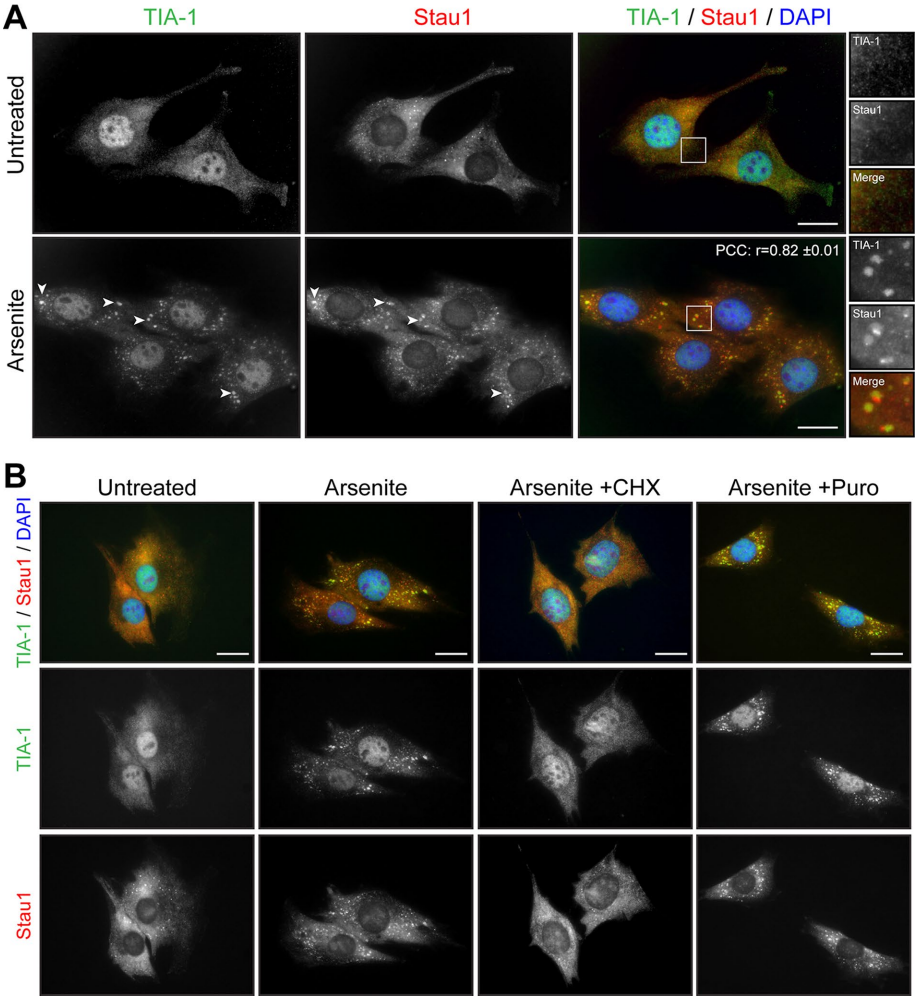

FIGURE 2: Staufen1 is recruited to SGs in Myoblasts. (A) Proliferative C2C12 myoblasts were untreated or treated with 0.5 mM arsenite for 45 min. Coimmunofluorescence staining was performed using Staufen1 and TIA-1 antibodies. (B) Proliferative C2C12 myoblasts were treated with CHX (50 µg/ml) or Puro (10 µg/ml) for the entire duration of the arsenite treatment and processed as in A. DAPI was used to stain nuclei. Arrowheads show SGs in myoblasts. Scale bars, 20 µm. For *r*, 18 cells were analyzed.

induces myoblasts to permanently withdraw from the cell cycle and initiate differentiation by fusing into elongated, multinucleated myotubes. Three-day-differentiated myotubes were treated with arsenite and SG formation assessed by TIA-1 and DDX3 immunofluorescence. Microscopy analyses showed that SGs form in multinucleated differentiated myotubes upon arsenite treatment ($r = 0.83 \pm 0.02$; Figure 4A). Pan–myosin heavy chain (MyHC) coimmunofluorescence was performed to identify differentiated myotubes from undifferentiated cells (Supplemental Figure S3). A pool of C2C12 reserve cells is known to escape from terminal differentiation and stay in a quiescent state alongside developing myotubes (Yoshida *et al.*, 1998). These quiescent reserve cells also form SGs after stress induction (Supplemental Figure S3) in a manner similar to that observed with proliferating myoblasts (Figure 1).

We next wondered whether Staufen1 is also recruited into SGs in differentiated mature myotubes. Three-day myotubes were treated with arsenite and assessed for TIA-1 and Staufen1 localization by immunofluorescence. We observed that in myotubes, Staufen1 is partially recruited into SGs, whereas a fraction of Staufen1 aggregates in the vicinity of SGs ($r = 0.76 \pm 0.02$; Figure 4B). Furthermore, C2C12 myoblasts were cotransfected with Staufen1-GFP and TIA-1–mCherry and differentiated for 3 d. When stressed with arsenite, Staufen1-GFP markedly aggregates into TIA-1-mCherry SGs in mature myotubes ($r = 0.73 \pm 0.02$; Figure 4C). Together these results show that the stress response pathway is conserved in mouse skeletal muscle cells since SGs can efficiently form in proliferative, quiescent, and differentiated muscle cells.

SG formation is specifically impaired in DM1 myoblasts

DM1 cells are under intracellular stress caused by expression of toxic mutant CUG^{exp} mRNAs (see *Introduction*). To investigate whether this RNA toxicity affects the stress response in DM1 cells, we first evaluated the formation of SGs in human primary fibroblast cells. We used three control (GM01653, GM03377, GM03523) and three DM1 primary cells carrying 50–80, 500, and 1700 CTG repeats (GM03991, GM03987, and GM03132, respectively). We induced SG formation with 0.5 mM arsenite as described with mouse C2C12 muscle cells.

We first studied TIA-1 and DDX3 localization in unstressed, control human primary fibroblasts (GM03377). By coimmunofluorescence, TIA-1 and DDX3 show a similar expression pattern, as also seen in mouse myoblasts. Indeed, we observed nuclear and lower cytoplasmic distribution for TIA-1 and more diffuse cytoplasmic staining for DDX3 (compare Figures 5A and 1A). Similar localization of TIA-1 and DDX3 was observed in other control fibroblasts (GM01653, GM03523), as well as in DM1 fibroblasts (GM03991, GM03987, GM03132), with no evidence of cytoplasmic aggregates of TIA-1 or DDX3 in absence of drug treatment (Supplemental Figure S4). This shows that toxic mutant DMPK mRNAs expressed in DM1 fibroblasts do not alone cause spontaneous formation of TIA-1 or DDX3 cytoplasmic granules.

We next analyzed how human primary fibroblasts respond to arsenic stress. After 45 min of arsenic treatment, distinct cytoplasmic, TIA-1/DDX3–positive SGs formed in stressed primary fibroblasts (Figure 5A). Signal intensity analyses over SGs along with high *r* (0.90 ± 0.01) show near-complete colocalization of TIA-1 and DDX3 in SGs (Supplemental Figure S1B). We also performed a thorough comparison of SG formation in control versus DM1 primary fibroblasts. Quantitative microscopy analyses using DDX3 as a marker revealed that the same ($p > 0.05$ for all conditions) number of SGs are formed between three controls and three human DM1 primary fibroblasts (Figure 5, B–D). In addition, the total SG area per cell (Figure 5E) and the mean SG size (Figure 5F) remained similar ($p > 0.05$ for all conditions) between controls and DM1 cells, showing that SGs form with the same efficiency in these cells despite expression of toxic mutant CUG^{exp} mRNAs.

Fibroblasts can be converted into myoblasts by MyoD expression (Davis *et al.*, 1987). To achieve this, we produced a lentivirus

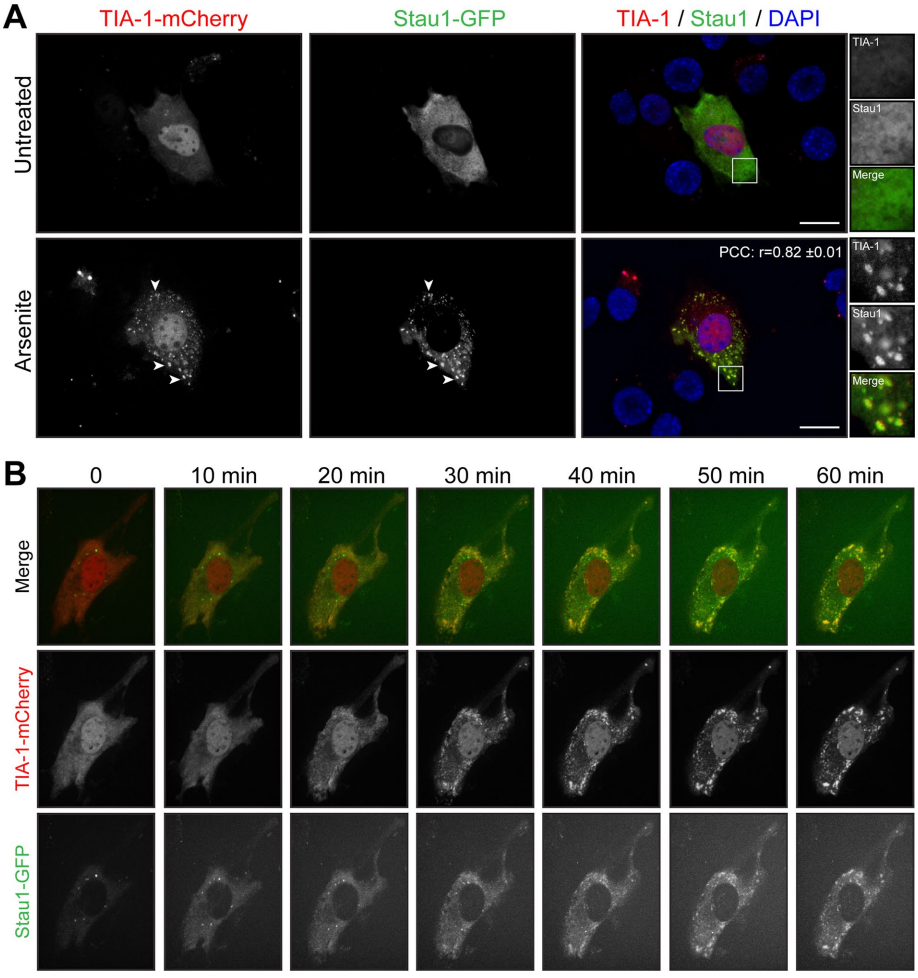

FIGURE 3: Staufen1 and TIA-1 are recruited concomitantly into SGs in myoblasts. (A) Proliferative C2C12 myoblasts were transfected with TIA-1-mCherry and Staufen1-GFP. Transfected cells were untreated or treated with 0.5 mM arsenite for 45 min. DAPI was used to stain nuclei. Arrowheads point to SGs. Right, magnifications of areas outlined by white boxes. Scale bars, 20 μm. For *r*, 18 cells were analyzed. (B) Time-lapse confocal microscopy using a spinning-disk confocal of transfected myoblasts after arsenite treatment (indicated time). Three independent experiments.

carrying an MyoD transgene and infected control and DM1 fibroblasts with lentivirus particles, as done previously (Ravel-Chapuis *et al.*, 2012). In parallel experiments, fibroblasts were infected with a control lentivirus expressing a GFP transgene to ensure that 100% of the cells were efficiently transduced under these conditions (Supplemental Figure S5). No evidence of cytoplasmic aggregate of TIA-1 or DDX3 was observed in MyoD-converted myoblasts in the absence of arsenite treatment (Supplemental Figure S6). Three days after infections, we assessed the formation of SGs in arsenite-treated control and DM1 MyoD-converted myoblasts by immunofluorescence using DDX3 antibodies. Our results show that SGs still form in control human myoblasts. However, after MyoD infection, SG formation is significantly impaired in the three DM1 myoblast cell lines tested compared with control cells ($p < 0.05$ vs. control GM01653 and GM03377 myoblasts, respectively; Figure 6, A–C). Accordingly, the total SG area was drastically decreased in the three DM1 cell lines cells ($p < 0.05$ vs. control GM01653 and GM03377 myoblasts, respectively; Figure 6D). However, the size of formed aggregates was unchanged between control and DM1 myoblasts ($p > 0.05$; Figure 6E), showing that when few individual SGs eventually form in DM1 myoblasts, they remain at a size equivalent to that of controls. Taken together, these results revealed that SG formation is markedly impaired in a cell type–specific manner.

The DM1 cell line GM03991 carries a low number of CTG repeats (50–80) normally associated with mild adult-onset symptoms. Here we observed a similar inhibition of SG formation in this cell line compared with other DM1 cells carrying longer expansions (500 and 1700). This may be related to the fact that these fibroblasts were harvested from an older DM1 patient displaying characteristic DM1 features (Table 1). Alternatively, this could also reflect the higher sensitivity of SG inhibition to low CTG repeats than alternative splicing defects.

Staufen1 down-regulation rescues SG formation in DM1 cells

We next investigated potential mechanisms involved in the cell type–specific inhibition of SG formation. DMPK gene expression is regulated by the MyoD myogenic regulatory factor through the binding to E-boxes present in its promoter (Storbeck *et al.*, 1998). To determine whether MyoD conversion of DM1 fibroblasts into myoblasts resulted in an increase in mutant CUG^{exp} mRNA expression, we measured total DMPK mRNA levels by quantitative reverse transcription PCR (qRT-PCR). As expected, we observed approximately twofold to fourfold increase in total DMPK level ($p < 0.05$) after MyoD overexpression (Figure 7A). Note that one control cell line (GM03523) showed a lower induction of DMPK mRNAs after MyoD conversion. This lower MyoD conversion, in fact, nicely correlates with the lower SG formation and likely accounts for the lower level of SGs in this wild-type cell line versus the other two controls (Figures 6, A, C, and D, and 7A).

We also performed FISH with Cy3-(CAG)10 probes to detect nuclear CUG^{exp} RNA foci. In our conditions, microscopy analysis showed that approximately three CUG^{exp} RNA foci per cell were in DM1 fibroblasts versus approximately five in MyoD-converted cells ($p < 0.001$; Figure 7, B and C). This increase in mutant DMPK mRNA sequestration mirrors the increase in DMPK mRNA expression induced by MyoD and cell conversion. However, the increase in RNA foci number is lower than the increase in the overall levels of DMPK mRNAs. This is likely because qRT-PCR measures both alleles of DMPK (normal and expanded), whereas FISH only highlights the nuclear accumulation of mutant DMPK transcripts (Figure 7, A–C).

We reported in our earlier work that the level of the RNA-binding protein Staufen1 is increased in vivo in muscles from three DM1 mouse models as well as in muscle biopsies from DM1 patients compared with controls (Ravel-Chapuis *et al.*, 2012). We thus assessed the level of Staufen1 in the various DM1 cells used in this study compared with controls. We performed Western blots on protein extracts obtained from proliferating control and DM1

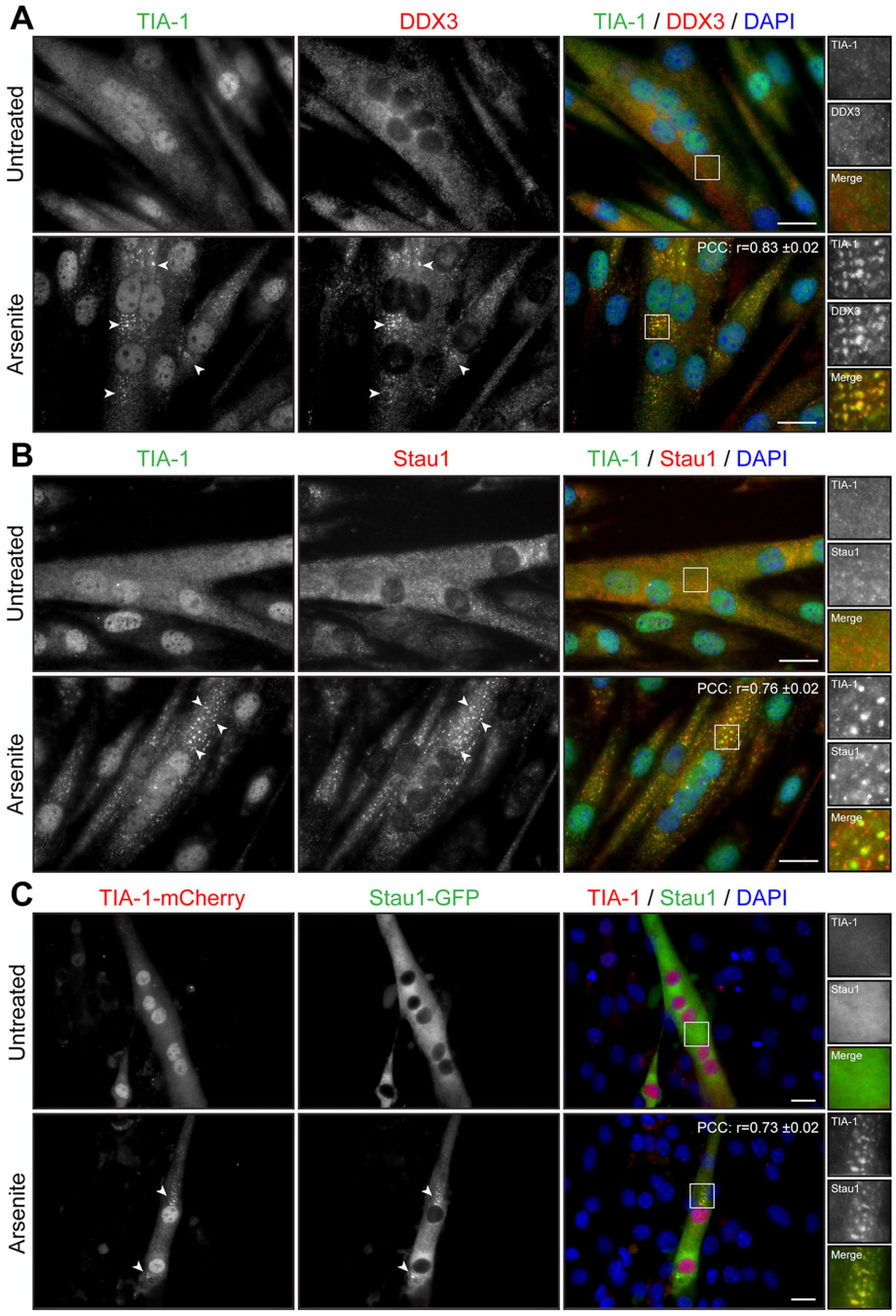

FIGURE 4: Arsenite induces formation of SGs in myotubes. (A, B) Three-day-differentiated myotubes were untreated or treated with 0.5 mM arsenite for 45 min. Coimmunofluorescence stainings were performed using TIA-1 and DDX3 or TIA-1 and Staufen1 antibodies. (C) C2C12 myoblasts transfected with TIA-1-mCherry and Staufen1-GFP were differentiated for 3 d. DAPI was used to stain nuclei. Arrowheads show SGs in myoblasts. Scale bars, 20 μm. For *r*, 9, 9, and 12 cells were analyzed, respectively.

fibroblasts and MyoD-converted myoblasts. Because fibroblasts and MyoD-converted cells were collected at different times, quantifications were expressed relative to their respective control cells. Results from wild-type control cells were pooled because no difference in Staufen1 and CUGBP1 expression levels were observed among the various cell lines (Supplemental Figure S7). First, such analyses revealed an increase in Staufen1 in GM03132 DM1 fibroblasts, which carry the largest CUG expansion (Figure 7, D and E). MyoD conversion only slightly increased Staufen1 levels in DM1 versus control myoblasts. Note that Staufen1 forms a doublet at ~55 kDa, as observed previously (Ravel-Chapuis *et al.*, 2012). Second, we measured CUGBP1 levels and observed an increase in GM03987 and GM03132 DM1 fibroblasts compared with control cells (Figure 7, D and E). In our conditions, we observed no increase in CUGBP1 steady-state levels in DM1 versus wild-type cells once they were MyoD converted. We did not observe any correlation between expression of total DMPK mRNA transcripts and Staufen1 or CUGBP1 levels (compare Figure 7, A vs. D and E). The most likely interpretation for this is that the increase in Staufen1 that we previously reported was observed in vivo with muscle tissue samples from mature DM1 mouse models and human patients (Ravel-Chapuis *et al.*, 2012). This increase, as we suggested in our earlier work, represents an adaptation to the DM pathology that likely requires a certain level of cellular maturity and a threshold in disease phenotype for it to happen. Such in vivo maturity- and disease stage–dependent effects can be only partially recapitulated in culture conditions.

Because Staufen1 is recruited to SGs in normal skeletal muscle cells (see earlier discussion), we wondered whether Staufen1 plays a role in SG formation in DM1 cells. To test this, we used a lentivirus expressing a specific Staufen1-targeting short hairpin RNA (shRNA). We recently showed that this lentivirus efficiently down-regulates endogenous Staufen1 protein levels in human primary muscle cells (Ravel-Chapuis *et al.*, 2014). Three days after infection, the degree of SG formation was assessed by immunofluorescence in control and Staufen1-depleted DM1 myoblasts after arsenite treatment. Microscopy analyses show that, as hypothesized, SG formation was increased in Staufen1-depleted DM1 cells compared with cells infected with a control lentivirus (Figure 8A). Quantitative analyses revealed a significant increase (p = 0.043 and 0.058) in two DM1 cell lines tested (GM03987, 500 CTG; and GM03132, 1700 CTG; Figure 8C). In a reverse experiment, we infected control human myoblasts (GM01653 and GM03377) with a lentivirus overexpressing a Staufen1 transgene or a control GFP. We observed a decrease in the total number of SGs in Staufen1-overexpressing cells (p = 0.0002 and 0.001 when comparing GM01653 and GM03377, respectively; Figure 8, B and D). In these experiments, the overexpression and knockdown of Staufen1 was verified by RT-PCR in both control and DM1 cells (Figure 8E). We conclude from these experiments that the modulation of Staufen1 levels regulates the efficiency of SG formation in DM1 cells.

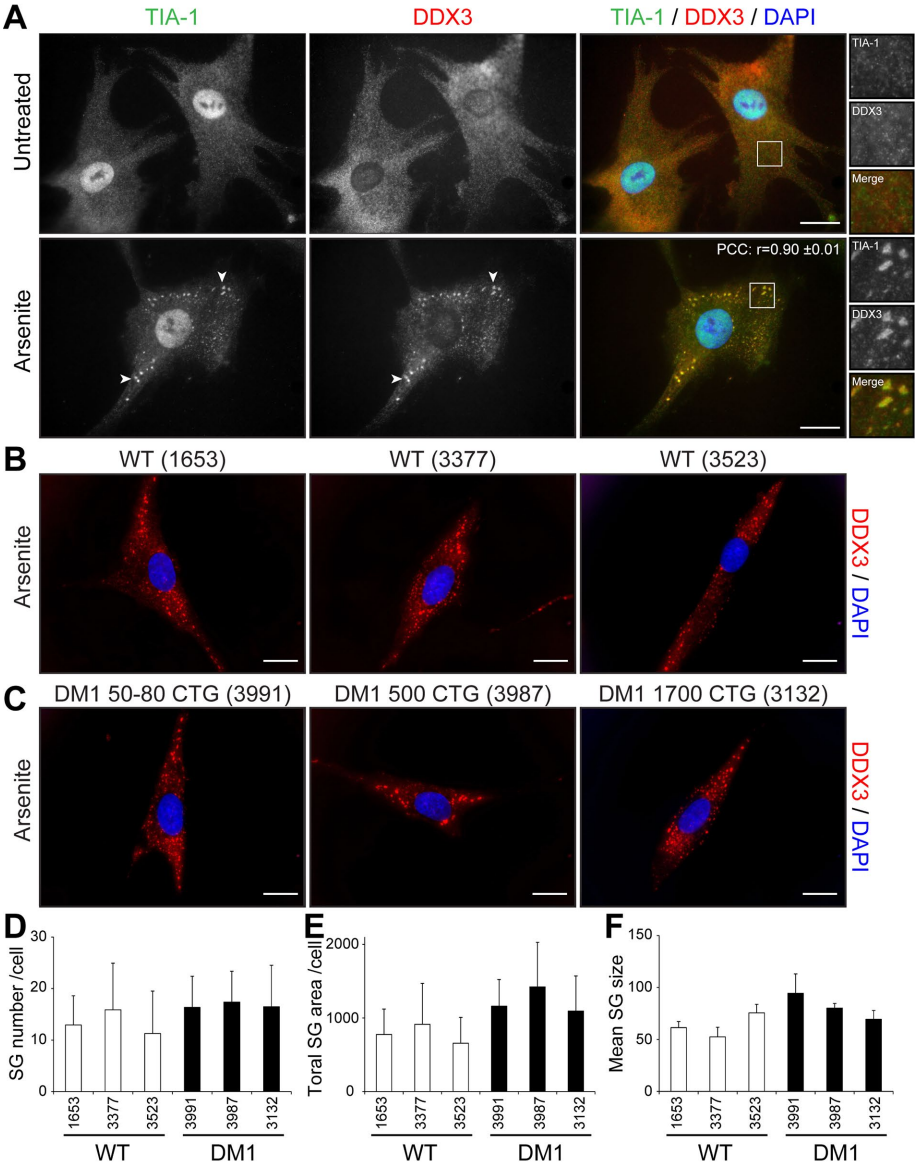

FIGURE 5: No difference was seen in SG formation between wild-type and human primary DM1 fibroblasts. (A) Human primary fibroblasts were untreated or treated with 0.5 mM arsenite for 45 min. Coimmunofluorescence staining was performed using TIA-1 and DDX3 antibodies. Arrowheads show SGs in human fibroblasts. Right, magnifications of areas outlined by white boxes. For *r*, 9 random cells were analyzed. Control (B) and DM1 (C) human primary fibroblasts were treated with 0.5 mM arsenite for 45 min. Immunofluorescence staining was performed using DDX3 antibodies to visualize SGs. The same exposure conditions were used to ensure quantitative analyses. DAPI was used to stain nuclei. Scale bars, 20 µm. (D) Mean number of SGs per cell, (E) total SG area (in pixels) per cell, and (F) mean SG size (pixels) per cell. From 117 to 174 random cells/condition were analyzed per condition in three independent experiments. ANOVA revealed no significant difference.

We first reported a novel role for Staufen1 in alternative splicing regulation, in particular insulin receptor (IR) splicing (Ravel-Chapuis *et al.*, 2012; Bondy-Chorney *et al.*, 2016). Indeed, we showed that Staufen1 overexpression promotes IR exon 11 inclusion in DM1 cells, thereby rescuing normal IR alternative splicing patterns. Here, in a reverse experiment, we further analyzed the effect of Staufen1 knockdown by shRNA on IR alternative splicing. First, we measured IR alternative splicing patterns in different DM1 cell lines by RT-PCR. As expected, we observed a CUG^{exp}-size-dependent increase in skipping of IR exon 11 compared with a control cell line (Figure 8E). Second, we show that Staufen1 depletion by shRNA in DM1 cells further promotes IR exon 11 skipping toward more severe DM1 phenotypes (Figure 8E). This confirms the major role played by Staufen1 in alternative splicing regulation and its protective role in IR alternative splicing in DM1. Together these findings indicate that Staufen1 participates in both the inhibition of SG formation and the regulation of IR alternative splicing. Our data thus show that Staufen1 is a crucial disease modifier in DM1, having multiple and opposite—beneficial and detrimental—roles in IR alternative splicing and SG formation, respectively.

DISCUSSION

In this study, we assessed the capacity of skeletal muscle cells to respond to stress by forming SGs. SGs are a large triage mRNA platform where stalled untranslated mRNA, multiple RNA-binding proteins, and molecules involved in diverse signaling pathways transiently accumulate in response to stress. SGs therefore form in cells in an attempt to adapt to and survive a transient stress (Kedersha *et al.*, 2013). We used the well-characterized TIA-1, DDX3, and PABP1 RNA-binding proteins as SGs markers to provide a detailed profile of SG formation in muscle cells. We showed the formation of distinct and characteristic cytoplasmic aggregates and near-perfect colocalization of SG markers in normal skeletal muscle cells in different states—proliferative, quiescent, and differentiated—in response to stressor exposure. Cytoplasmic granules containing SG markers have been described in muscle cells, but information concerning their specific nature was fragmentary (Polesskaya *et al.*, 2007; Huichalaf *et al.*, 2010; Di Marco *et al.*, 2012; van der Laan *et al.*, 2012).

Normal skeletal muscle cells are subject to a variety of stress conditions, including mechanical stress during muscle contraction, oxidative stress due to the generation of free radicals, and ER stress (Kuwahara *et al.*, 2010; Castrogiovanni and Imbesi, 2012; Rayavarapu *et al.*, 2012; Deldicque, 2013). Our results showing that myoblasts can efficiently form SGs in response to oxidative stress and ER stress are therefore important because they show that skeletal muscle cells possess protective mechanisms to cope with these various stressors. Of particular interest, we found here that the RNA-binding protein Staufen1 is also recruited to SGs in skeletal muscle cells. The presence of Staufen1 in SGs has been reported in primary rat oligodendrocytes (Thomas *et al.*, 2005) and NIH3T3, HeLa, and BHK immortalized cell lines (Thomas *et al.*, 2009) but never, to our knowledge, in skeletal muscle cells.

It is well documented that DM1 is caused by RNA toxicity. Expression of the mutant CUG^{exp} mRNA leads to an imbalance in

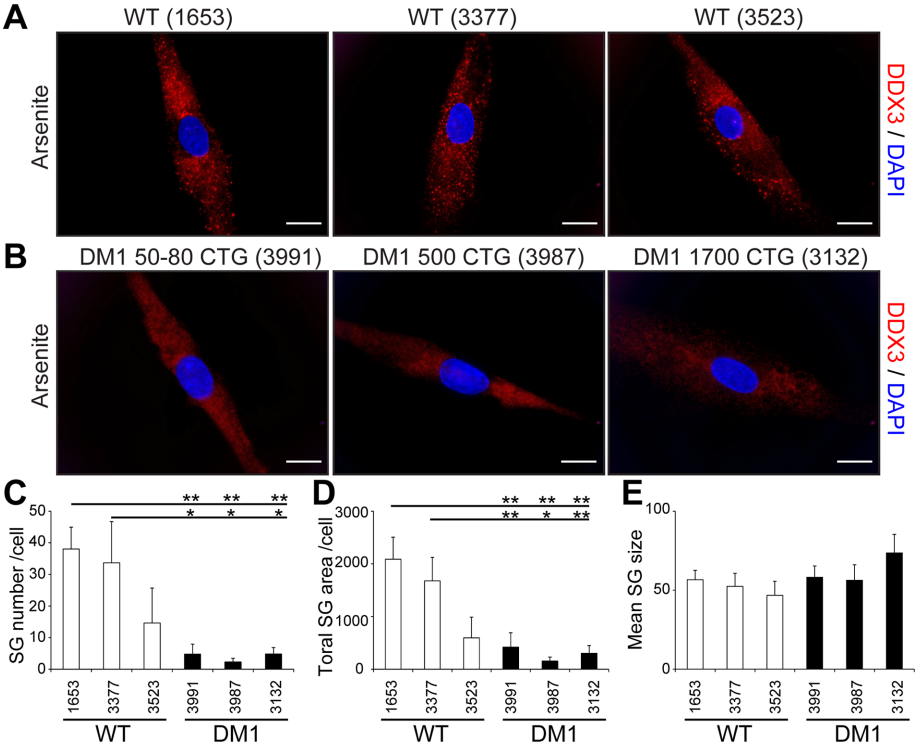

FIGURE 6: Impaired SG formation in DM1 myoblasts. Control (A) and DM1 (B) human primary fibroblasts were converted into myoblasts by MyoD-lentivirus infections. Three days after infections, myoblasts were treated with 0.5 mM arsenite for 45 min. Immunofluorescence was performed with DDX3 antibodies to visualize SGs. DAPI was used to stain nuclei. The same exposure conditions were used to ensure quantitative analyses. Scale bars, 20 μm. (C) Mean number of SGs per cell, (D) total SG area (in pixels) per cell, and (E) mean SG size (pixels) per cell. From 134 to 179 random cells/condition were analyzed in three independent experiments. ANOVA was performed, and asterisks indicate significance (*$p \leq 0.05$ and **$p \leq 0.01$).

the expression of multiple RNA-binding proteins, including MBNL1, CUGBP1, and Staufen1. These proteins are known splicing regulators, so their imbalance modifies alternative splicing of key pre-mRNAs, causing some of the main symptoms of DM1, such as insulin resistance and myotonia (Savkur *et al.*, 2001; Charlet *et al.*, 2002; Yamashita *et al.*, 2012). It has become evident that other aspects of RNA metabolism are also perturbed by the misregulation of these RNA-binding proteins. Studies have shown that miRNA biogenesis and mRNA stability and translation are also affected in the disease (Schoser and Timchenko, 2010; Mahadevan, 2012). Therefore DM1 appears as an even more complex disorder, with many aspects of RNA metabolism being perturbed. Here we add to this complexity by showing that the potential of DM1 myoblasts to respond to stress by forming SGs is reduced and that Staufen1 participates in this regulation.

Our present findings led us to propose that Staufen1 participates in the etiology of the DM1 disorder at least in part by decreasing the ability of DM1 cells to survive the stress generated by expression of the toxic CUG^{exp} mRNA. Huichalaf *et al.* (2010) reported that CUG^{exp} causes stress to DM1 cells, activating a double-stranded RNA–dependent protein kinase (PKR)-eIF2α signaling pathway and promoting the accumulation of inactive CUGBP1-eIF2α complexes into SGs, resulting in the inhibition of specific CUGBP1 translational mRNA targets in SGs. In addition, they showed that DM1 myoblasts display increased cytoplasmic TIA-1 staining in the absence of external stress stimulation (Huichalaf *et al.*, 2010). Here, however, we failed to observe any increase in TIA-1 or DDX3 cytoplasmic staining in untreated DM1 fibroblasts or MyoD-converted myoblasts in culture. This discrepancy could be attributed to differences in the origin of the cells used in these studies. Together such findings nonetheless reinforce the fact that the stress response is clearly affected in DM1 cells and that the combined action of Staufen1 and CUGBP1 on SGs participates in the etiology of DM1.

In the present study, we thus unraveled a novel cellular event that likely participates in DM1 pathogenesis in skeletal muscles. Indeed, we showed that the potential of DM1 myoblasts to respond to stress by forming SGs is reduced and that Staufen1 participates in this repression. Very little is known about the role of SGs in normal skeletal muscle physiology and neuromuscular disorders. Two groups have reported that a point mutation in the coding region of TIA-1 is the primary cause of a rare adult-onset autosomal disorder called Welander distal myopathy (WDM; Hackman *et al.*, 2013; Klar *et al.*, 2013). Immunostaining of patient biopsies revealed the increase of TIA-1 staining in vacuoles present in skeletal muscle fibers that are characteristic of the disease. The molecular consequences of this specific mutation in TIA-1 remain to be elucidated,

Cell line	Cell type	CTG repeats	Sex	Age at sampling (yr)	Symptoms
GM01653	Healthy	N/A	Male	37	N/A
GM03377	Healthy	N/A	Male	19	N/A
GM03523	Healthy	N/A	Male	21	N/A
GM03991	DM1	50–80	Female	76	Distal weakness, cataracts, clinical and electrical (electromyography) myotonia, and frontal baldness
GM03987	DM1	500	Male	39	Distal weakness, clinical and electrical myotonia, cataracts, and marked balding
GM03132	DM1	1700	Male	18	Bone deformities, muscle wasting, and myotonia

Coriell Cell Repositories, Coriell Institute for Medical Research, Camden, NJ.

TABLE 1: Control and DM1 human fibroblasts.

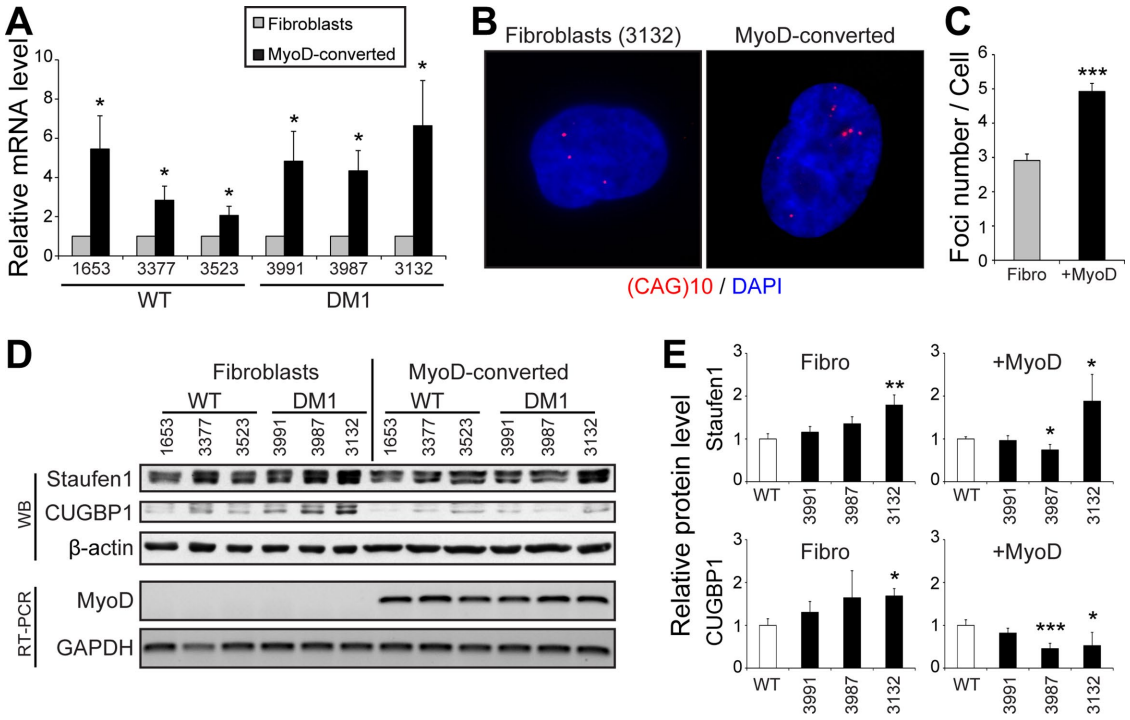

FIGURE 7: MyoD-conversion induces DMPK expression and aggregation in DM1 cells. (A) Relative quantification of DMPK mRNA levels in fibroblasts and MyoD-converted myoblasts as determined by qRT-PCR. Three independent experiments. (B) FISH of control human DM1 primary fibroblasts and MyoD-converted myoblasts (GM03132, 1700 CTG) using a Cy3-(CAG)10 probe. (C) Quantifications of FISH experiments. From 40 to 57 random cells/condition were analyzed. (D) Top, Western blots showing Staufen1 and CUGBP1 protein levels in wild-type and DM1 fibroblasts and MyoD-converted myoblasts. β-Actin was used as a loading control. Bottom, relative quantification of MyoD mRNA levels as determined by RT-PCR. GAPDH was used to show equal loading. (E) Quantifications of Staufen1 and CUGBP1 levels normalized to GAPDH. Three or four independent experiments. Student's *t* tests were used, and asterisks indicate significance (*$p \leq 0.05$, **$p \leq 0.01$, and ***$p \leq 0.001$).

but an altered response to stress in WDM muscle cells may be expected.

A link between SGs and neurodegenerative disorders has been proposed. Many protein components of RNA granules are recruited to and modulate formation of SGs, including TAR DNA-binding protein 43 (TDP-43), Fused in Sarcoma (FUS), Survival of Motor Neuron (SMN), fragile X mental retardation protein (FMRP), and ataxin-2 (Buchan, 2014). Mutations in these RNA-binding proteins or their misregulation contribute to neuronal cell dysfunctions and are believed to be the primary cause of various neurodegenerative disorders. Staufen1 is a well-known component of cytoplasmic RNA granules in neuronal cells (Krichevsky and Kosik, 2001). Mice lacking functional Staufen1 show defects in dendritic mRNA transport and neuron morphology (Vessey *et al.*, 2008). Staufen1 forms a complex with TDP-43 and FMRP proteins, as they coimmunoprecipitate in both SH-SY5Y neuroblastoma and HEK293T embryonic kidney cell lines (Yu *et al.*, 2012). In addition, Staufen1 colocalizes with FMRP in *Drosophila* neuronal RNA granules and with TDP-43 in control and amyotrophic lateral sclerosis (ALS)–affected spinal motor neurons (Barbee *et al.*, 2006; Volkening *et al.*, 2009). This raises the possibility that in addition to its role in DM1 skeletal muscle, Staufen1 is also potentially involved in neurodegenerative disorders such as Alzheimer's disease, ALS, and fragile X syndrome. Furthermore, DM1 is a multisystemic disorder, and patients with DM1 display cognitive dysfunctions and intraneuronal aggregates of hyperphosphorylated Tau proteins in their CNS, connecting DM1 to the group of neurodegenerative diseases (Sergeant *et al.*, 2001). Perturbations in Staufen1 levels or activity in DM1 neurons might alter one or several of the functions of Staufen1, such as alternative splicing, RNA granule transport, and/or stress response, which would implicate Staufen1 in the DM1 neuronal physiopathology in addition to its role in skeletal muscle.

MATERIALS AND METHODS

Antibodies

The antibodies used were anti-DDX3 (Bethyl Laboratories/Cederlane, Burlington, Canada), anti-TIA1 and anti-CUGBP1 (Santa Cruz Biotechnology, Santa Cruz, CA), anti-PABP1 (Cell Signalling/New England Biolabs, Whitby, Canada), anti-Staufen1 and anti–glyceraldehyde-3-phosphate dehydrogenase (GAPDH; Abcam/Cederlane), and anti-MyHC (MF20; Developmental Studies Hybridoma Bank, Iowa City, IA).

Cell culture conditions and stress granule formation

C2C12 cells (American Type Culture Collection/Cederlane) were maintained in growth medium (DMEM, 10% fetal bovine serum [Wisent Bioproducts, St-Bruno, Canada], 100 U/ml penicillin, and 100 µg/ml streptomycin). To induce myogenic differentiation, C2C12 cells were allowed to become confluent on Matrigel-coated (BD Biosciences/Fisher Scientific) plates, and the medium was switched to differentiation medium (DMEM, 2% horse serum [PAA Laboratories, Piscataway, NJ], 100 U/ml penicillin, and 100 µg/ml streptomycin). Control (GM01653, GM03377, GM03523) and DM1 (GM03991, GM03987, GM03132) human fibroblasts (Coriell Cell Repositories, Coriell Institute for Medical Research, Camden, NJ; Table 1) were grown according to instructions.

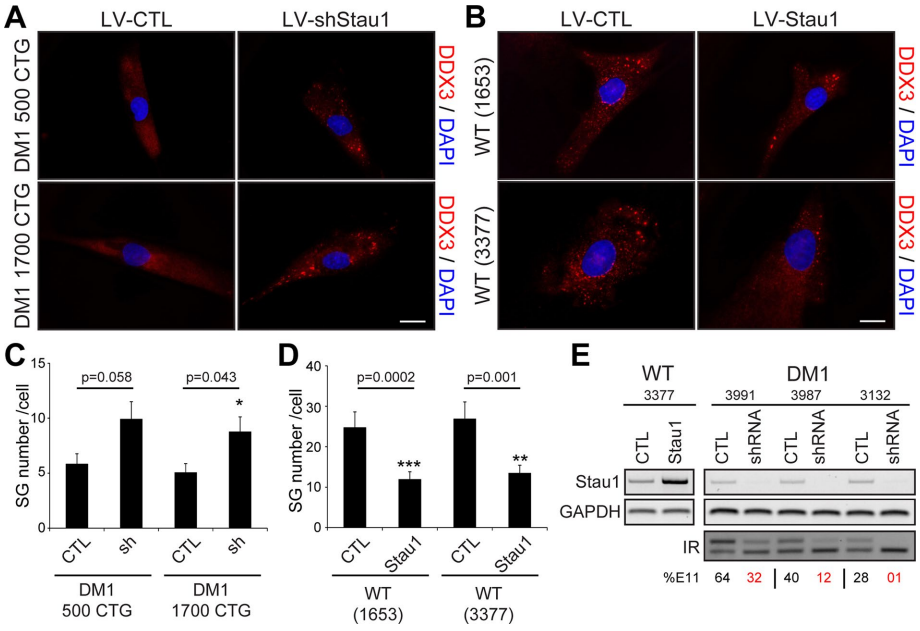

FIGURE 8: Rescue of stress granule formation by Staufen1 down-regulation in DM1 myoblasts. (A) Human DM1 primary myoblasts (GM03987, 500 CTG; and GM03132, 1700 CTG) were infected with a control lentivirus or a specific Staufen1 shRNA. Three days after transductions, cells were treated with 0.5 mM arsenite for 45 min. Immunofluorescence was performed with DDX3 antibodies to visualize SGs. (B) Wild-type primary myoblasts (GM01653 and GM03377) were infected with a control lentivirus expressing GFP or a lentivirus overexpressing Staufen1. Cells were then processed as in A. DAPI was used to stain nuclei. The same exposure conditions were used to ensure quantitative analyses. Scale bars, 20 µm. (C, D) Mean number of SGs per cell. A total of 40 random cells per condition were analyzed. Student's *t* tests were used, and asterisks indicate significance (*$p \leq 0.05$, **$p \leq 0.01$, and ***$p \leq 0.001$). (E) Top, relative quantification of Staufen1 mRNA levels as determined by RT-PCR showing up-regulation or knockdown of Staufen1 after lentivirus infections. GAPDH was used to show equal loading. Bottom, IR alternative splicing profiles were assessed by RT-PCR. Numbers show the percentage of IR exon 11 inclusion.

Induction of SG formation was done by treating cells with 0.5 mM arsenite (Sigma-Aldrich, Oakville, Canada) for 45 min at 37°C. Alternatively, SG formation was also induced using 1 µM thapsigargin (Sigma-Aldrich) for 60 min at 37°C or by heat shock for 45 min at 45°C. When specified, C2C12 cells were treated with CHX (50 µg/ml; Sigma-Aldrich) or puromycin (Puro, 10 µg/ml; Wisent Bioproducts) just before and for the entire duration of the arsenite treatment.

Lentivirus production and infections

pCDH-MyoD vector was obtained by subcloning MyoD cDNA from pBRIT-MyoD into pCDH-CMV-MCS-EF1-copGFP (System Biosciences/Cederlane). pCDH, pCDH-MyoD, pCDH-Stau1 (Ravel-Chapuis *et al.*, 2012), plKO.1, and plKO.1-shStau1 plasmids (Open Biosystems GE Dharmacon/Fisher Scientific) were used as lentivectors. Lentiviral particles were produced by transient transfection of 293T cells with lentivectors along with psPax2 and pMD2.G packaging plasmids. The conditioned medium containing viral particles was collected and used to transduce primary cells overnight in the presence of 6 µg/ml Polybrene (Sigma-Aldrich). Infected cells were grown for 3–5 d before analyses.

Immunofluorescence

Cells were fixed for 15 min in 1× phosphate-buffered saline (PBS) and 4% formaldehyde. Cells were permeabilized for 10 min with methanol at –20°C. Cells were rinsed with 1× PBS and blocked with blocking buffer (1× PBS, 1% bovine serum albumin [BSA], and 0.1% Triton). Cells were incubated with the primary antibody diluted in blocking buffer for 1 h at 37°C or overnight at 4°C. Then the cells were thoroughly washed with 1× PBS and incubated for 1 h with Alexa secondary antibodies diluted in blocking buffer (Invitrogen Life Technologies/Fisher Scientific). Slides were mounted with Vectashield mounting medium (Vector Labs/Cederlane) containing 4′,6-diamidino-2-phenylindole (DAPI) for staining of nuclei. Fluorescent images were visualized on a Zeiss Axio Imager.M2 microscope equipped with Zeiss 63× Plan-Apochromat 1.4 oil, 40× Plan-Apochromat 1.4 oil, and 20× Plan-Apochromat 0.8 objective lenses. Images were acquired with a Zeiss AxioCam MRm detector and processed with the Zeiss AxioVision software, Photoshop CS5 (Abobe Systems, San Jose, CA), or ImageJ (National Institutes of Health, Bethesda, MD).

For SG analysis, a constant exposure time was used during image acquisition to ensure comparison between the different conditions. Image analyses were performed using ImageJ software. A threshold value was fixed to a number allowing a good visualization of SGs over the background in a control arsenite-treated condition and kept constant for all images. Longer exposure time resulted in an increase in background without affecting the measurement. SG number and size were then determined using the Analyze Particles module with a size threshold fixed at 10 to infinity. For SG analysis in human fibroblasts and MyoD-converted cells 117–179 random cells/condition were analyzed in three independent experiments. For up-regulation and knockdown of Staufen1 experiments, 40 random cells/condition were analyzed. For colocalization analysis, Pearson's *r* was calculated using the Coloc 2 ImageJ plug-in. A region of interest corresponding to the whole cytoplasmic area was selected for *r* quantifications.

Live-cell imaging

C2C12 cells were transfected with Staufen1-GFP (Wickham *et al.*, 1999) and TIA-1-mCherry (derived from pEYFP-TIA-1, kindly provided by Nancy Kedersha, Harvard Medical School and Brigham and Women's Hospital, Boston, MA) plasmids using Lipofectamine Plus reagent (Invitrogen Life Technologies/Fisher Scientific) according to the manufacturer's instructions. At 24 h later, 100,000 cells were plated on cell imaging dishes (Eppendorf/Fisher Scientific). At 48 h after transfection, cells were imaged in phenol red–free medium on a spinning-disk confocal microscope (Quorum Technologies, Guelph, Canada) with inverted stand equipped with an environmental-controlled chamber (temperature, humidifier, and CO_2) and 40× 1.3 oil PL APO objective lens. Images were acquired with an electron-multiplying charge-coupled device ImagEM detector (Hamamatsu/Quorum Technologies) and MetaMorph software (Molecular Devices/Quorum Technologies). Image acquisitions were performed every 5 min for 1 h after arsenite addition. Twenty *z*-stacks were taken for each channel and each time point. A total of

16 random cells from three independent experiments were imaged. Images were processed with ImageJ.

RNA fluorescence in situ hybridization

FISH was performed as previously described (Ravel-Chapuis *et al.*, 2012). Briefly, cells were covered with 40% formamide and 2× saline–sodium citrate (SSC) for 10 min and incubated for 2 h with 10 ng of Cy3-labeled (CAG)10 oligonucleotide probe in hybridization buffer (40% formamide, 2× SSC, 0.2% BSA, 10% dextran sulfate, 2 mM vanadyl adenosine complex, 1 mg/ml tRNA, and salmon sperm DNA). After washes, slides were mounted with Vectashield medium containing DAPI (Vector Labs) and visualized and analyzed as in the *Immunofluorescence* section. From 40 to 57 random cells/condition were analyzed.

RNA extraction, reverse transcription, and real-time quantitative PCR

Total RNAs were extracted from samples using TRIzol (Invitrogen Life Technologies/Fisher Scientific) or TriPure (Roche/Sigma-Aldrich). A 1-µg amount of RNA was DNase-treated (Ambion/ThermoFisher Scientific, Ottawa, Canada), and cDNAs were synthesized using MuLV Reverse Transcriptase (Applied Biosystems/ThermoFisher Scientific). mRNA expression was evaluated by real-time quantitative PCR (MX3005P; Stratagene/Agilent Technologies, Santa Clara, CA) using the QuantiTect SYBR Green PCR Kit (Qiagen, Toronto, Canada) according to the manufacturer's instructions. The sequences of the primers were, for h-DMPK, forward, 5′-CCGTTGGAAGACTGAGTGC-3′, and reverse, 5′-CATTCCCGGCTACAAGGAC-3′). Results were normalized to at least three reference genes: GAPDH, SDHA, HMBS, or RPLI3A (Vandesompele *et al.*, 2002). PCRs were performed using GoTaq (Promega/Fisher Scientific) according to manufacturer's instructions. The sequences of the primers were as follows: for h-Staufen1, forward, 5′-CGGAACTTGCCTGTGAATTT-3′, and reverse, 5′-CCAGTTGCTCAGAGGGTCTC-3′); for m-MyoD, forward, 5′-TGGCATGATGGATTACAGCG′, and reverse, 5′-CCACTATGCTGGACAGGCAGT-3′); for h-GAPDH, forward, 5′-TGCACCACCAACTGCTTAGC-3′, and reverse, 5′-GGCATGGACTGTGGTCATGAG-3′); and for h-IR, forward, 5′-CCAAAGACAGACTCTCAGAT-3′, and reverse, 5′-AACATCGCCAAGGGACCTGC-3′.

Western blotting

Cells were resuspended in urea/thiourea buffer (7 M urea, 2 M thiourea, 65 mM 3-[(3-cholamidopropyl)dimethylammonio]-1-propanesulfonate, 100 mM dithiothreitol, 10 U of DNase I, and protease inhibitors [Complete; Roche/Sigma-Aldrich]), and the protein concentration was determined using the CB-X Protein Assay kit (G-Bioscience, St. Louis, MO). A 20-µg amount of total proteins was separated by SDS–PAGE and transferred onto nitrocellulose membranes. Nonspecific binding was first blocked with 1× PBS containing 5% skim milk, and membranes were then incubated with primary antibodies. After thorough washing with 1× PBS with 0.05% Tween, membranes were incubated with horseradish peroxidase–conjugated secondary antibodies (Jackson Immunoresearch Laboratories/Cederlane). After washes, signals were revealed using ECL reagents (Fisher Scientific) and autoradiographed with x-ray films (Fisher Scientific).

Statistical analysis

Student's *t* tests and analysis of variance (ANOVA) were used to determine whether differences between groups were significant. The level of significance was set at $p \leq 0.05$. *$p \leq 0.05$, **$p \leq 0.01$, and ***$p \leq 0.001$. Means ± SEM are presented throughout, unless otherwise specified.

ACKNOWLEDGMENTS

We thank C. Péladeau and J. Lunde for technical assistance and A. Fanous for generating the TIA-1-mCherry construct. This work was supported by the Canadian Institutes of Health Research, the Association Française contre les Myopathies, and the Muscular Dystrophy Association. J.C. was the recipient of the Canada Research Chair (Tier II) in RNA Metabolism funded through the Canadian Institutes of Health Research.

REFERENCES

Anderson P, Kedersha N (2008). Stress granules: the Tao of RNA triage. Trends Biochem Sci 33, 141–150.

Barbee SA, Estes PS, Cziko AM, Hillebrand J, Luedeman RA, Coller JM, Johnson N, Howlett IC, Geng C, Ueda R, *et al.* (2006). Staufen- and FMRP-containing neuronal RNPs are structurally and functionally related to somatic P bodies. Neuron 52, 997–1009.

Belanger G, Stocksley MA, Vandromme M, Schaeffer L, Furic L, DesGroseillers L, Jasmin BJ (2003). Localization of the RNA-binding proteins Staufen1 and Staufen2 at the mammalian neuromuscular junction. J Neurochem 86, 669–677.

Bondy-Chorney E, Crawford Parks TE, Ravel-Chapuis A, Klinck R, Rocheleau L, Pelchat M, Chabot B, Jasmin BJ, Côté J (2016). Staufen1 regulates multiple alternative splicing events either positively or negatively in DM1 indicating its role as a disease modifier. PLoS Genet 12, e1005827.

Botta A, Malena A, Loro E, Del Moro G, Suman M, Pantic B, Szabadkai G, Vergani L (2013). Altered Ca2 +homeostasis and endoplasmic reticulum stress in myotonic dystrophy type 1 muscle cells. Genes (Basel) 4, 275–292.

Buchan JR (2014). mRNP granules: assembly, function, and connections with disease. RNA Biol 11, 1019–1030.

Buchan JR, Parker R (2009). Eukaryotic stress granules: the ins and outs of translation. Mol Cell 36, 932–941.

Castrogiovanni P, Imbesi R (2012). Oxidative stress and skeletal muscle in exercise. Ital J Anat Embryol 117, 107–117.

Charlet BN, Savkur RS, Singh G, Philips AV, Grice EA, Cooper TA (2002). Loss of the muscle-specific chloride channel in type 1 myotonic dystrophy due to misregulated alternative splicing. Mol Cell 10, 45–53.

Dang Y, Kedersha N, Low WK, Romo D, Gorospe M, Kaufman R, Anderson P, Liu JO (2006). Eukaryotic initiation factor 2alpha-independent pathway of stress granule induction by the natural product pateamine A. J Biol Chem 281, 32870–32878.

Davis RL, Weintraub H, Lassar AB (1987). Expression of a single transfected cDNA converts fibroblasts to myoblasts. Cell 51, 987–1000.

Deldicque L (2013). Endoplasmic reticulum stress in human skeletal muscle: any contribution to sarcopenia? Front Physiol 4, 236.

Di Marco S, Cammas A, Lian XJ, Kovacs EN, Ma JF, Hall DT, Mazroui R, Richardson J, Pelletier J, Gallouzi IE (2012). The translation inhibitor pateamine A prevents cachexia-induced muscle wasting in mice. Nat Commun 3, 896.

Farny NG, Kedersha NL, Silver PA (2009). Metazoan stress granule assembly is mediated by P-eIF2alpha-dependent and -independent mechanisms. RNA 15, 1814–1821.

Fu YH, Pizzuti A, Fenwick RG Jr, King J, Rajnarayan S, Dunne PW, Dubel J, Nasser GA, Ashizawa T, de Jong P, *et al.* (1992). An unstable triplet repeat in a gene related to myotonic muscular dystrophy. Science 255, 1256–1258.

Gilks N, Kedersha N, Ayodele M, Shen L, Stoecklin G, Dember LM, Anderson P (2004). Stress granule assembly is mediated by prion-like aggregation of TIA-1. Mol Biol Cell 15, 5383–5398.

Goulet I, Boisvenue S, Mokas S, Mazroui R, Cote J (2008). TDRD3, a novel Tudor domain-containing protein, localizes to cytoplasmic stress granules. Hum Mol Genet 17, 3055–3074.

Hackman P, Sarparanta J, Lehtinen S, Vihola A, Evila A, Jonson PH, Luque H, Kere J, Screen M, Chinnery PF, *et al.* (2013). Welander distal myopathy is caused by a mutation in the RNA-binding protein TIA1. Ann Neurol 73, 500–509.

Huichalaf C, Sakai K, Jin B, Jones K, Wang GL, Schoser B, Schneider-Gold C, Sarkar P, Pereira-Smith OM, Timchenko N, *et al.* (2010). Expansion of CUG RNA repeats causes stress and inhibition of translation in myotonic dystrophy 1 (DM1) cells. FASEB J 24, 3706–3719.

Ihara Y, Mori A, Hayabara T, Namba R, Nobukuni K, Sato K, Miyata S, Edamatsu R, Liu J, Kawai M (1995). Free radicals, lipid peroxides and

antioxidants in blood of patients with myotonic dystrophy. J Neurol 242, 119–122.
Ikezoe K, Nakamori M, Furuya H, Arahata H, Kanemoto S, Kimura T, Imaizumi K, Takahashi MP, Sakoda S, Fujii N, *et al.* (2007). Endoplasmic reticulum stress in myotonic dystrophy type 1 muscle. Acta Neuropathol 114, 527–535.
Kedersha N, Anderson P (2007). Mammalian stress granules and processing bodies. Methods Enzymol 431, 61–81.
Kedersha N, Cho MR, Li W, Yacono PW, Chen S, Gilks N, Golan DE, Anderson P (2000). Dynamic shuttling of TIA-1 accompanies the recruitment of mRNA to mammalian stress granules. J Cell Biol 151, 1257–1268.
Kedersha NL, Gupta M, Li W, Miller I, Anderson P (1999). RNA-binding proteins TIA-1 and TIAR link the phosphorylation of eIF-2 alpha to the assembly of mammalian stress granules. J Cell Biol 147, 1431–1442.
Kedersha N, Ivanov P, Anderson P (2013). Stress granules and cell signaling: more than just a passing phase? Trends Biochem Sci 38, 494–506.
Kedersha N, Stoecklin G, Ayodele M, Yacono P, Lykke-Andersen J, Fritzler MJ, Scheuner D, Kaufman RJ, Golan DE, Anderson P (2005). Stress granules and processing bodies are dynamically linked sites of mRNP remodeling. J Cell Biol 169, 871–884.
Klar J, Sobol M, Melberg A, Mabert K, Ameur A, Johansson AC, Feuk L, Entesarian M, Orlen H, Casar-Borota O, *et al.* (2013). Welander distal myopathy caused by an ancient founder mutation in TIA1 associated with perturbed splicing. Hum Mutat 34, 572–577.
Krichevsky AM, Kosik KS (2001). Neuronal RNA granules: a link between RNA localization and stimulation-dependent translation. Neuron 32, 683–696.
Kumar A, Kumar V, Singh SK, Muthuswamy S, Agarwal S (2014). Imbalanced oxidant and antioxidant ratio in myotonic dystrophy type 1. Free Radic Res 48, 503–510.
Kuwahara H, Horie T, Ishikawa S, Tsuda C, Kawakami S, Noda Y, Kaneko T, Tahara S, Tachibana T, Okabe M, *et al.* (2010). Oxidative stress in skeletal muscle causes severe disturbance of exercise activity without muscle atrophy. Free Radic Biol Med 48, 1252–1262.
Lai MC, Lee YH, Tarn WY (2008). The DEAD-box RNA helicase DDX3 associates with export messenger ribonucleoproteins as well as tip-associated protein and participates in translational control. Mol Biol Cell 19, 3847–3858.
Mahadevan MS (2012). Myotonic dystrophy: is a narrow focus obscuring the rest of the field? Curr Opin Neurol 25, 609–613.
Mazroui R, Sukarieh R, Bordeleau ME, Kaufman RJ, Northcote P, Tanaka J, Gallouzi I, Pelletier J (2006). Inhibition of ribosome recruitment induces stress granule formation independently of eukaryotic initiation factor 2alpha phosphorylation. Mol Biol Cell 17, 4212–4219.
Miller JW, Urbinati CR, Teng-Umnuay P, Stenberg MG, Byrne BJ, Thornton CA, Swanson MS (2000). Recruitment of human muscleblind proteins to (CUG)(n) expansions associated with myotonic dystrophy. EMBO J 19, 4439–4448.
Mokas S, Mills JR, Garreau C, Fournier MJ, Robert F, Arya P, Kaufman RJ, Pelletier J, Mazroui R (2009). Uncoupling stress granule assembly and translation initiation inhibition. Mol Biol Cell 20, 2673–2683.
Polesskaya A, Cuvellier S, Naguibneva I, Duquet A, Moss EG, Harel-Bellan A (2007). Lin-28 binds IGF-2 mRNA and participates in skeletal myogenesis by increasing translation efficiency. Genes Dev 21, 1125–1138.
Ravel-Chapuis A, Belanger G, Yadava RS, Mahadevan MS, Desgroseillers L, Cote J, Jasmin BJ (2012). The RNA-binding protein Staufen1 is increased in DM1 skeletal muscle and promotes alternative pre-mRNA splicing. J Cell Biol 196, 699–712.
Ravel-Chapuis A, Crawford TE, Blais-Crepeau ML, Belanger G, Richer CT, Jasmin BJ (2014). The RNA-binding protein Staufen1 impairs myogenic differentiation via a c-myc-dependent mechanism. Mol Biol Cell 25, 3765–3778.
Rayavarapu S, Coley W, Nagaraju K (2012). Endoplasmic reticulum stress in skeletal muscle homeostasis and disease. Curr Rheumatol Rep 14, 238–243.
Savkur RS, Philips AV, Cooper TA (2001). Aberrant regulation of insulin receptor alternative splicing is associated with insulin resistance in myotonic dystrophy. Nat Genet 29, 40–47.
Schoser B, Timchenko L (2010). Myotonic dystrophies 1 and 2: complex diseases with complex mechanisms. Curr Genomics 11, 77–90.
Sergeant N, Sablonniere B, Schraen-Maschke S, Ghestem A, Maurage CA, Wattez A, Vermersch P, Delacourte A (2001). Dysregulation of human brain microtubule-associated tau mRNA maturation in myotonic dystrophy type 1. Hum Mol Genet 10, 2143–2155.
Shih JW, Wang WT, Tsai TY, Kuo CY, Li HK, Wu Lee YH (2012). Critical roles of RNA helicase DDX3 and its interactions with eIF4E/PABP1 in stress granule assembly and stress response. Biochem J 441, 119–129.
Storbeck CJ, Sabourin LA, Waring JD, Korneluk RG (1998). Definition of regulatory sequence elements in the promoter region and the first intron of the myotonic dystrophy protein kinase gene. J Biol Chem 273, 9139–9147.
Thomas MG, Tosar LJ, Desbats MA, Leishman CC, Boccaccio GL (2009). Mammalian Staufen 1 is recruited to stress granules and impairs their assembly. J Cell Sci 122, 563–573.
Thomas MG, Martinez Tosar LJ, Loschi M, Pasquini JM, Correale J, Kindler S, Boccaccio GL (2005). Staufen recruitment into stress granules does not affect early mRNA transport in oligodendrocytes. Mol Biol Cell 16, 405–420.
Thornton CA (2014). Myotonic dystrophy. Neurol Clin 32, 705–719.
Toscano A, Messina S, Campo GM, Di Leo R, Musumeci O, Rodolico C, Aguennouz M, Annesi G, Messina C, Vita G (2005). Oxidative stress in myotonic dystrophy type 1. Free Radic Res 39, 771–776.
Tourriere H, Chebli K, Zekri L, Courselaud B, Blanchard JM, Bertrand E, Tazi J (2003). The RasGAP-associated endoribonuclease G3BP assembles stress granules. J Cell Biol 160, 823–831.
Tsilfidis C, MacKenzie AE, Mettler G, Barcelo J, Korneluk RG (1992). Correlation between CTG trinucleotide repeat length and frequency of severe congenital myotonic dystrophy. Nat Genet 1, 192–195.
Usuki F, Ishiura S (1998). Expanded CTG repeats in myotonin protein kinase increase susceptibility to oxidative stress. Neuroreport 9, 2291–2296.
Usuki F, Takahashi N, Sasagawa N, Ishiura S (2000). Differential signaling pathways following oxidative stress in mutant myotonin protein kinase cDNA-transfected C2C12 cell lines. Biochem Biophys Res Commun 267, 739–743.
van der Laan AM, van Gemert AM, Dirks RW, Noordermeer JN, Fradkin LG, Tanke HJ, Jost CR (2012). mRNA cycles through hypoxia-induced stress granules in live Drosophila embryonic muscles. Int J Dev Biol 56, 701–709.
Vandesompele J, De Preter K, Pattyn F, Poppe B, Van Roy N, De Paepe A, Speleman F (2002). Accurate normalization of real-time quantitative RT-PCR data by geometric averaging of multiple internal control genes. Genome Biol 3, RESEARCH0034.
Vessey JP, Macchi P, Stein JM, Mikl M, Hawker KN, Vogelsang P, Wieczorek K, Vendra G, Riefler J, Tubing F, *et al.* (2008). A loss of function allele for murine Staufen1 leads to impairment of dendritic Staufen1-RNP delivery and dendritic spine morphogenesis. Proc Natl Acad Sci USA 105, 16374–16379.
Volkening K, Leystra-Lantz C, Yang W, Jaffee H, Strong MJ (2009). Tar DNA binding protein of 43 kDa (TDP-43), 14-3-3 proteins and copper/zinc superoxide dismutase (SOD1) interact to modulate NFL mRNA stability. Implications for altered RNA processing in amyotrophic lateral sclerosis (ALS). Brain Res 1305, 168–182.
Wickham L, Duchaine T, Luo M, Nabi IR, DesGroseillers L (1999). Mammalian staufen is a double-stranded-RNA- and tubulin-binding protein which localizes to the rough endoplasmic reticulum. Mol Cell Biol 19, 2220–2230.
Yamashita Y, Matsuura T, Shinmi J, Amakusa Y, Masuda A, Ito M, Kinoshita M, Furuya H, Abe K, Ibi T, *et al.* (2012). Four parameters increase the sensitivity and specificity of the exon array analysis and disclose 25 novel aberrantly spliced exons in myotonic dystrophy. J Hum Genet 57, 368–374.
Yoshida N, Yoshida S, Koishi K, Masuda K, Nabeshima Y (1998). Cell heterogeneity upon myogenic differentiation: down-regulation of MyoD and Myf-5 generates "reserve cells." J Cell Sci 111, 769–779.
Yu Z, Fan D, Gui B, Shi L, Xuan C, Shan L, Wang Q, Shang Y, Wang Y (2012). Neurodegeneration-associated TDP-43 interacts with fragile X mental retardation protein (FMRP)/Staufen (STAU1) and regulates SIRT1 expression in neuronal cells. J Biol Chem 287, 22560–22572.